Nondestructive Testing and Evaluation,
Vol. 24, Nos. 1–2, March–June 2009, 209–232

Taylor & Francis
Taylor & Francis Group

Eddy current residual stress profiling in surface-treated engine alloys

Bassam A. Abu-Nabah[a1], Feng Yu[a2], Waled T. Hassan[b3], Mark P. Blodgett[c] and Peter B. Nagy[a]*

[a]*Department of Aerospace Engineering, University of Cincinnati, Cincinnati, OH 45221, USA;* [b]*Honeywell Aerospace, Phoenix, AZ 85034, USA;* [c]*Air Force Research Laboratory, WPAFB, Dayton, OH 45433, USA*

(*Received 3 June 2008; final version received 3 June 2008*)

Recent research results indicate that eddy current conductivity measurements can be exploited for nondestructive evaluation of subsurface residual stresses in surface-treated nickel-base superalloy components. According to this approach, the depth-dependent electric conductivity profile is calculated from the measured frequency-dependent apparent eddy current conductivity spectrum. Then, the residual stress depth profile is calculated from the conductivity profile based on the piezoresistivity coefficient of the material, which is determined separately from calibration measurements using the known external applied stresses. This paper reviews the basic principles, measurement procedures, advantages, and limitations of eddy current residual stress profiling.

Keywords: eddy current; spectroscopy; surface-treatment; residual stress profiling

1. Introduction

Nondestructive residual stress assessment in fracture-critical components is one of the most promising opportunities and difficult challenges we face in the NDE community today. Residual stress assessment is important because there is mounting evidence that it is not possible to reliably and accurately predict the remaining service life of such components without properly accounting for the presence of residual stresses. Unfortunately, both the absolute level and spatial distribution of the residual stress are rather uncertain, partly because the stress is highly susceptible to variations in the manufacturing process and subsequently it tends to undergo thermo-mechanical relaxation at operating temperatures. Therefore, the only reliable way to establish the actual level and spatial profile of the prevailing residual stress is by measuring them. Unfortunately, the only currently available NDE method for residual stress assessment is based on X-ray diffraction (XRD) measurement that is limited to an extremely thin, less than 20 μm deep, surface layer [1–4]. In this study, to get the necessary information on the subsurface residual stresses destructive XRD measurements were conducted on selected specimens following the nondestructive eddy current conductivity measurements. The XRD method is routinely used to measure subsurface residual stresses via repeated removal of thin surface layers by electro-polishing. When such layer removal is performed, the measured stress needs to be corrected for the stress relaxation and redistribution that occurs because of layer removal [5,6].

The peak diffraction direction is determined by the absolute elastic strain in the material. At the same time, as a by-product of this measurement, we also get some information on the plastic deformation in the material because the widening of the diffraction peak is due to the lack of periodicity in the lattice, which is related to dislocation density and other lattice

*Corresponding author. Email: peter.nagy@uc.edu

ISSN 1058-9759 print/ISSN 1477-2671 online

DOI: 10.1080/10589750802245280
http://www.informaworld.com

Report Documentation Page

Form Approved
OMB No. 0704-0188

1. REPORT DATE	2. REPORT TYPE	3. DATES COVERED
2009		**00-00-2009 to 00-00-2009**

4. TITLE AND SUBTITLE	5a. CONTRACT NUMBER
Eddy current residual stress profiling in surface-treated engine alloys	5b. GRANT NUMBER
	5c. PROGRAM ELEMENT NUMBER
6. AUTHOR(S)	5d. PROJECT NUMBER
	5e. TASK NUMBER
	5f. WORK UNIT NUMBER
7. PERFORMING ORGANIZATION NAME(S) AND ADDRESS(ES) **Department of Aerospace Engineering,University of Cincinnati,Cincinnati,OH,45221**	8. PERFORMING ORGANIZATION REPORT NUMBER
9. SPONSORING/MONITORING AGENCY NAME(S) AND ADDRESS(ES)	10. SPONSOR/MONITOR'S ACRONYM(S)
	11. SPONSOR/MONITOR'S REPORT NUMBER(S)

12. DISTRIBUTION/AVAILABILITY STATEMENT
Approved for public release; distribution unlimited

13. SUPPLEMENTARY NOTES

14. ABSTRACT

15. SUBJECT TERMS

16. SECURITY CLASSIFICATION OF:			17. LIMITATION OF ABSTRACT	18. NUMBER OF PAGES	19a. NAME OF RESPONSIBLE PERSON
a. REPORT	b. ABSTRACT	c. THIS PAGE			
unclassified	**unclassified**	**unclassified**	**Same as Report (SAR)**	**24**	

imperfections. However, in order to evaluate the whole compressive part of the subsurface residual stress profile using XRD measurements, successive layer removal has to be applied, which requires some numerical corrections to account for the inevitable stress release during this process. This method is inherently destructive since it leaves a deep hole on the surface. Although the accuracy of XRD measurements is quite sufficient for life prediction purposes, the necessity of surface layer removal for subsurface measurements essentially excludes the use of this method as a nondestructive characterisation tool.

There are really only two ways to avoid this limitation of XRD, namely either by increasing the incident beam intensity or by reducing the wave length, which then reduces the X-ray absorption coefficient of the material so that one gets better penetration. Today, this can be achieved only by using either synchrotron radiation or neutron diffraction, which could increase the penetration depth to a few centimetres [7,8]. On the negative side, the spatial resolution of these methods leaves much to be desired since a minimum diffraction volume must be maintained to reach sufficient sensitivity and that translates into a depth resolution on the order of 100 μm. That is still enough, although barely, for surface-treated components, even for shot-peened ones which exhibit rather shallow compressive residual stress layers. Of course, it is a major disadvantage of these techniques that they require access to a synchrotron accelerator or a nuclear reactor.

Surface enhancement methods, such as shot peening (SP), laser shock peening (LSP), and low-plasticity burnishing (LPB), significantly improve the fatigue resistance and foreign object damage tolerance of metallic components by introducing beneficial near-surface compressive residual stresses. Moreover, the surface is slightly strengthened and hardened by the cold-working process. By far the most common way to produce protective surface layers of compressive residual stress is by SP, though it is probably also the worst technique from the point of view of damaging cold work which substantially decreases the thermo-mechanical stability of the microstructure at elevated operating temperatures and leads to accelerated relaxation of the beneficial residual stresses [2]. Although LSP and LPB produces significiantly deeper compressive residual stress than SP, their main advantage over SP is that they produce much less cold work on the order of 5–15% equivalent plastic strain.

2. Eddy current conductivity spectroscopy

Because of the above discussed limitations, the NDE community has been looking for alternatives to assess residual stress profiles in surface-treated engine components for many years and eddy current conductivity spectroscopy emerged as one of the leading candidates [9–28]. Eddy current residual stress profiling is based on the piezoresistivity of the material, i.e., on the characteristic dependence of the electric conductivity on stress. Figure 1 shows a schematic representation of physics-based eddy current residual stress profiling in surface-treated components. In order to remove the influence of the measurement system (coil size, shape, etc.) the actually measured complex electric impedance of the probe coil is first transformed into a so-called apparent eddy current conductivity (AECC) parameter. At a given inspection frequency, the AECC is defined as the electric conductivity of an equivalent homogeneous, non-magnetic, smooth, and flat specimen placed at a properly chosen distance from the coil that would produce the same complex electric coil impedance as the inhomogeneous specimen under study [19].

If spurious material (e.g., magnetic permeability) and geometric (e.g., surface roughness) variations can be neglected, the frequency-dependent AECC can be inverted for the depth-dependent electric conductivity profile (this principal path is highlighted in Figure 1). Then, using the known piezoresistivity of the material, the sought residual stress profile can be calculated. Unfortunately, the measured complex electric coil impedance, and therefore also the

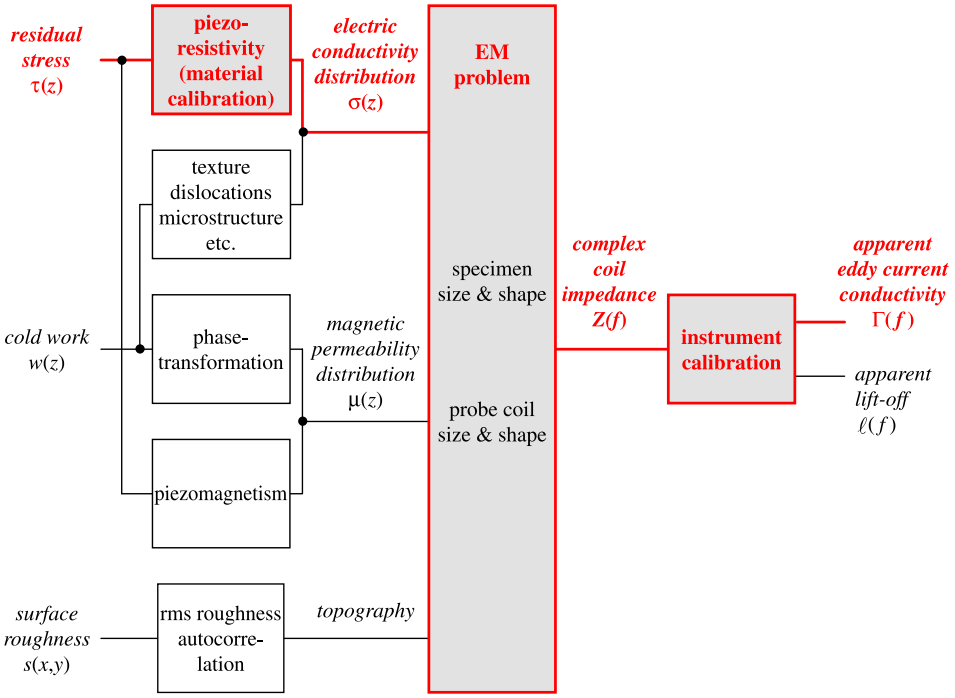

Figure 1. A schematic representation of physics-based eddy current residual stress profiling in surface-treated components (the principal path is highlighted).

inferred AECC, is affected by the presence of cold work and surface roughness as well as by the sought near-surface residual stress. The electric conductivity variation due to residual stress is usually weak (≈1%) and rather difficult to separate from these accompanying spurious effects. In certain materials, such as austenitic stainless steels, cold work might also cause significant magnetic permeability variation which affects the measured coil impedance. Fortunately, nickel-base superalloys do not exhibit such ferromagnetic transition from their paramagnetic state [22]. In addition, because of their significant hardness, shot-peened nickel-base superalloy components exhibit only rather limited surface roughness (≈2–3 μm rms), therefore the influence of geometrical irregularities is also limited. Still, as the inspection frequency increases the eddy current loop becomes squeezed closer to the rough surface, which creates a more tortuous, therefore longer, path and might lead to a perceivable drop of AECC above 30–40 MHz [29–31].

In order to translate the measured frequency-dependent AECC into a depth-dependent electric conductivity profile in a non-magnetic medium, first a simplistic inversion technique was developed [20], which was recently followed by the development of a highly convergent iterative inversion technique [23]. Both techniques indicated that at any given frequency the measured AECC corresponds roughly to the actual electric conductivity at half of the standard penetration depth assuming that: (i) the electric conductivity variation is limited to a shallow surface region of depth much less than the probe coil diameter, (ii) the relative change in electric conductivity is less than a few percents, and (iii) the electric conductivity depth profile is continuous and fairly smooth. Alternatively, best fitting of the measured electric coil impedance with the known analytical solution can be used assuming that the conductivity profile can be characterised by a small number of independent parameters [28]. Finally, the sought residual

stress profile is calculated from the electric conductivity profile based on the piezoresistivity coefficient of the material, which is determined separately from the material calibration measurements using the known external applied stresses.

2.1 Material calibration, piezoresistivity

In the presence of elastic stress τ the electrical conductivity σ tensor of an isotropic conductor becomes slightly anisotropic. In general, the stress-dependence of the electrical resistivity can be described by the fourth-order piezoresistivity tensor [32–38]. In direct analogy to the well-known acoustoelastic coefficients, the widely used NDE terminology for the stress coefficient of the acoustic velocity, the stress coefficient of the electrical conductivity is referred to as the electroelastic coefficient.

$$\begin{bmatrix} \Delta\sigma_1/\sigma_0 \\ \Delta\sigma_2/\sigma_0 \\ \Delta\sigma_3/\sigma_0 \end{bmatrix} = \begin{bmatrix} \kappa_{11} & \kappa_{12} & \kappa_{12} \\ \kappa_{12} & \kappa_{11} & \kappa_{12} \\ \kappa_{12} & \kappa_{12} & \kappa_{11} \end{bmatrix} \begin{bmatrix} \tau_1/E \\ \tau_2/E \\ \tau_3/E \end{bmatrix}. \quad (1)$$

Here, E denotes Young's modulus, $\Delta\sigma_i = \sigma_i - \sigma_0\,(i = 1,2,3)$ denotes the conductivity change due to the presence of stress, σ_0 denotes the electrical conductivity in the absence of stress, and κ_{11} and κ_{12} are the unitless parallel and normal electroelastic coefficients, respectively. During materials calibration, directional racetrack [39] or meanderising [40] probe coils can be used to measure the parallel κ_{11} and normal κ_{12} electroelastic coefficients essentially independent of each other. In the case of shot-peened or otherwise treated surfaces, essentially isotropic plane stress ($\tau_1 = \tau_2 = \tau_{ip}$ and $\tau_3 = 0$) condition prevails. Then, regardless whether conventional non-directional circular or directional probes are used, the effective electroelastic coefficient is $\kappa_{ip} = \kappa_{11} + \kappa_{12}$.

As it was illustrated in Figure 1, the electric conductivity is sensitive to both elastic strains caused by the prevailing residual stress state and plastic strains produced by prior cold work, i.e., it lacks the selectivity to separate these two principal effects of surface treatment. This is rather unfortunate, but not unusual at all in nondestructive evaluation which often has to rely on indirect measurements to remain nondestructive. Since the effects of cold work and associated microstructural changes are not fully understood at this point, the electric conductivity depth profiles will be converted into estimated residual stress profiles based solely on the piezoelectric effect according to equation (1). It will be shown that completely neglecting cold work effects causes a systematic error in the estimated residual stress profiles. The simplest way to account for cold work effects is to use empirically corrected electroelastic coefficients instead of the calibration values independently measured under purely elastic deformation [21]. The necessary empirical correction then indicates the relative contribution of the otherwise unaccounted for cold work effects rather than the uncertainty of the electroelastic coefficient obtained by calibration.

Figure 2 shows examples of piezoresistivity measurements in Waspaloy, IN718, and Ti–6Al–4V engine materials using a directional eddy current probe parallel and normal to the applied uniaxial load. Here, the normalised change in conductivity $\Delta\sigma/\sigma_0$ is plotted against the uniaxial strain $\varepsilon_{ua} = \tau_{ua}/E$. In some materials, such as Ti–6Al–4V, the parallel and normal electroelastic coefficients are more or less equal in magnitude and opposite in sign, which renders the eddy current conductivity measurements essentially useless for residual stress assessment in the case of isotropic plane stress on surface-treated components. However, there is a very important group of materials, notably nickel-base superalloys, where the two coefficients have similar magnitudes and signs, therefore the parallel and normal effects reinforce each other to produce a fairly significant stress-dependence. In order to quantitatively assess the prevailing

residual stress from eddy current conductivity measurements, the electroelastic coefficients of the material must be first determined using known external applied stresses. These calibration measurements are usually conducted on a reference specimen of the same material using cyclic uniaxial loads between 0.1 and 10 Hz, which is fast enough to produce adiabatic conditions. It was shown that such dynamic calibration measurements should be corrected for the thermoelastic effect, which is always positive, i.e., it increases the conductivity in tension, when the material cools down, and reduces it in compression, when the material heats up [21]. For high-conductivity alloys the difference between the adiabatic and isothermal properties could be as high as 50%. However, for high-temperature engine alloys of low electrical conductivity, such as nickel-base superalloys and titanium alloys, the difference between the isothermal and adiabatic parameters is fairly low at $\approx 5-10\%$.

In paramagnetic materials, the electric conductivity increases by approximately 1% under a maximum biaxial compressive stress equal to the yield strength of the material. Still, it was found that in shot-peened aluminium and titanium alloy specimens the measured AECC typically decreases as much as 1–2% with increasing peening intensity, which indicates that cold work and surface roughness effects dominate the observed phenomenon [15–17,19]. Figure 3 illustrates that, in sharp contrast with most other materials, intact (solid symbols) shot-peened nickel-base superalloys exhibit a relative increase in AECC both with increasing peening intensity as well as with increasing inspection frequency [19]. Furthermore, the excess AECC completely vanishes upon full thermal relaxation (empty symbols) in spite of the fact that some remnant cold work is still present in the specimens. These results also illustrate that in nickel-base superalloys the slight surface roughness produced by SP does not cause a perceivable drop of AECC up to at least 10 MHz.

There is, however, a significant problem with the very promising eddy current results shown in Figure 3. Based on the independently measured piezoresistivity effect of the material, the observed AECC increase is significantly higher than it should be if the effect were solely due to the residual stress (elastic strain) contribution. It was found that this overestimation is mainly due to the uncorrected effect of cold work (plastic strain) that also increases the electric conductivity in severely peened components [22]. Because of the reduced thermo-mechanical stability of near-surface residual stress in the presence of excessive cold work, engine

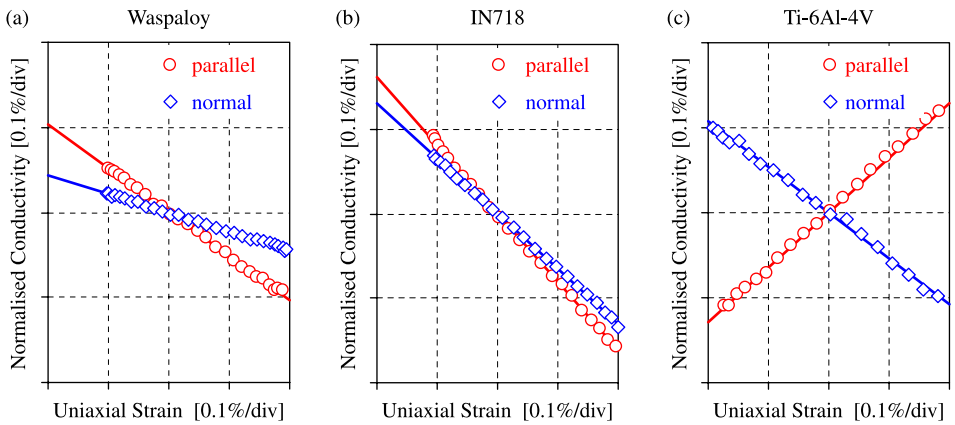

Figure 2. Piezoresistivity measurements in Waspaloy (a), IN 718 (b) and Ti–6Al–4V (c) using a directional eddy current probe parallel and normal to the applied uniaxial load.

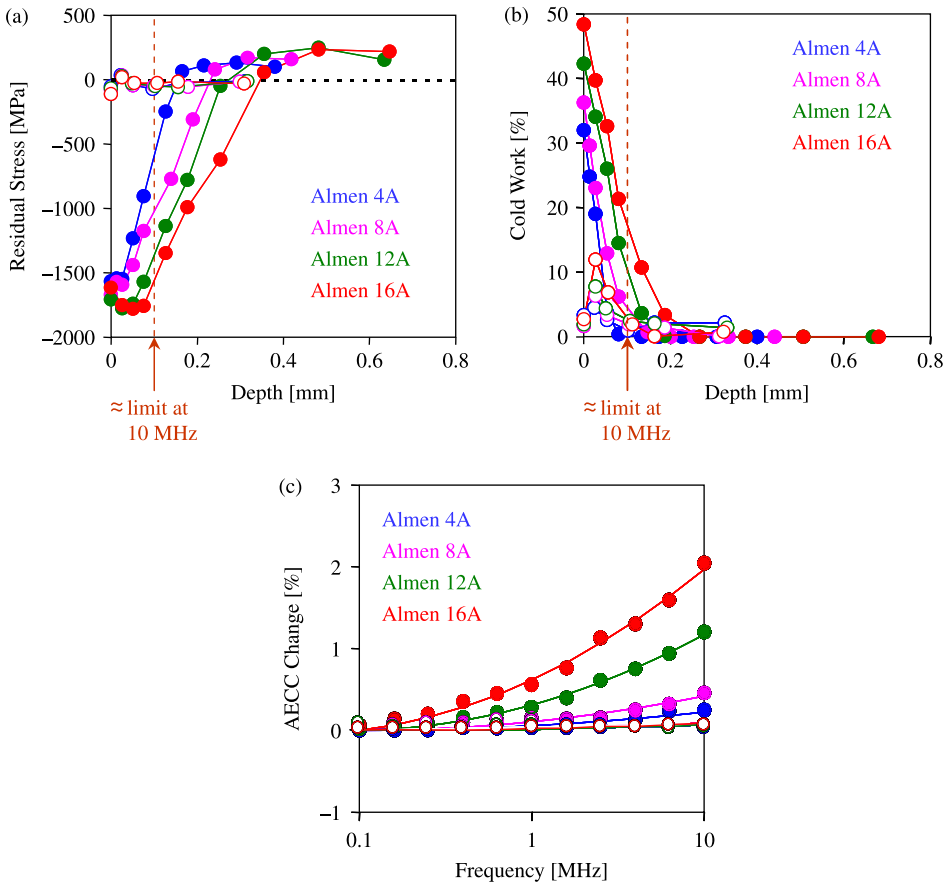

Figure 3. XRD residual stress (a) and cold work (b) depth profiles and AECC change (c) in shot-peened Waspaloy specimens before (solid circles) and after (empty circles) full stress relaxation at 900°C for 24 h.

manufacturers refrain from using peening intensities above Almen 8A anyway, therefore the overestimation caused by excessive cold work is of limited concern. However, if the Almen 12A and 16A peening intensities were removed from Figure 3, the remaining AECC effect would be almost buried in experimental uncertainties, which clearly indicates that lower peening intensities cannot be properly characterised without increasing the inspection frequency above 10 MHz. Knowing the electric conductivity of the intact material and the approximate depth of the near-surface conductivity profile allows us to determine the inspection frequency range required to retrieve the depth-dependent electric conductivity profile from the measured frequency-dependent AECC spectrum. In particular, to capture the near-surface hook of the residual stress profile in shot-peened nickel-base superalloys the frequency range of inspection has to be extended far beyond 10 MHz, where the effective inspection depth is only $\approx 100\,\mu$m, as it is illustrated by the vertical dashed lines in Figure 3. In subsequent sections, we will illustrate that moderately peened specimens of acceptable cold work levels (Almen 6A or less) require special high-frequency inspection procedures while in specimens of high SP intensity (above Almen 6A) the influence of cold work on the electric conductivity of the material cannot be neglected.

2.2 Instrument calibration

Most eddy current inspections are conducted in one of two basic modes of operation, namely in 'impedance' and 'conductivity' modes. In the so-called conductivity mode, which is most often used for alloy sorting and quantitative characterisation of metals, the measured probe coil impedance is evaluated for an 'apparent' eddy current conductivity $\Gamma(f)$ and 'apparent' lift-off distance $\ell(f)$ by assuming that the specimen is a sufficiently large homogeneous non-magnetic conductor, even when it is actually not. At a given frequency f and hypothetical lift-off distance $\ell(f)$, a hypothetical material of conductivity $\Gamma(f)$ would produce exactly the same complex coil impedance as the real specimen under test. Complications such as inhomogeneity, permeability effects, surface roughness, etc., are neglected during inversion of the coil impedance, therefore the thereby measured quantity will be referred to as AECC. Existing differences between the actual specimen and an ideal homogeneous non-magnetic conductor exert a convoluted effect on the measured AECC and make it frequency-dependent. Of course, the intrinsic electrical conductivity of the material is independent of frequency. In the case of layered or otherwise inhomogeneous specimens the observed frequency-dependence of the AECC is due to the depth-dependence of the electrical conductivity or magnetic permeability and the frequency-dependence of the eddy current penetration depth. Furthermore, near-surface defects and spurious surface roughness could also cause an additional frequency-dependent loss of eddy current conductivity.

For a given set of vertical and horizontal gains and phase rotation, the real and imaginary components of the measured complex impedance are determined by the electric conductivity of the specimen and the lift-off distance. For the purposes of instrument calibration, four reference points are measured on two appropriate calibration blocks (σ_1 and σ_2) with ($\ell = s$) and without ($\ell = 0$) a polymer foil of thickness s between the probe coil and the specimens. The coil impedance measured on the shot-peened specimen is then evaluated in terms of apparent conductivity and lift-off using simple linear interpolation, though the lift-off data is often discarded. It should be mentioned that the linear interpolation technique, which is known to leave much to be desired over larger conductivity ranges, is quite sufficient over the relatively small range considered in this study unless the inspection frequency exceeds 20 MHz. Later, we will show that at high inspection frequencies efficient rejection of inevitable lift-off variations is of the utmost importance because of the high precision requirements of these measurements and better lift-off rejection requires nonlinear interpolation.

In the conductivity mode of operation, the measured frequency-dependent complex electric impedance of the coil is first translated into an AECC spectrum as it was shown schematically in Figure 1, which is then inverted into a frequency-independent depth profile of the electric conductivity, as it will be shown in the next section. The main advantage of this two-step approach is that it effectively eliminates the influence of the measurement system on the actually measured coil impedance, therefore AECC spectra taken with different equipments and different probe coils can be directly compared. To illustrate the robustness of this instrument calibration method, Figure 4 shows the AECC spectra measured by four different instruments (Nortec 2000S, Agilent 4294A, Stanford Research SR844, and UniWest US-450) on three IN718 specimens of different peening intensities. In the overlapping frequency ranges the agreement between the AECC spectra obtained by different instruments is within the respective estimated errors of the instruments. Of course, true physical quantities do not depend on the way they are measured. However, eddy current conductivity measurements are inherently susceptible to influence by the measurement system because of the complex relationship between the true material parameter, i.e., the depth-dependent electric conductivity, and the measured physical parameter, i.e., the frequency-dependent AECC. Independence of the measured AECC from the

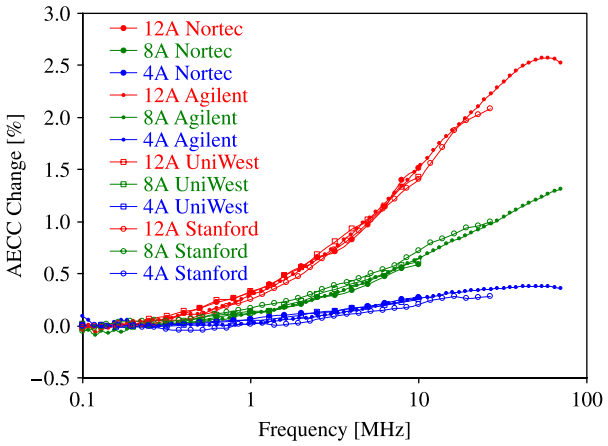

Figure 4. AECC change measured by four different instruments (Nortec 2000S, Agilent 4294A, Stanford Research SR844, and UniWest US-450) on three IN718 specimens of different peening intensities.

influence of the measurement system is a necessary condition for the use of physics-based inversion models, which is an integral part of the method taken in our study.

Up to 10 MHz, commercially available absolute pancake and pencil probes can be used for AECC measurements. The frequency bandwidth of such probes is limited to typically less than one decade because of the very high sensitivity and stability requirements of eddy current residual stress profiling. Above 10 MHz, flexible spiral coils can be used to minimise the adverse self- and stray-capacitance effects [27]. The spiral coils used in our study had separate transmit and receive coils that increases their thermal stability by eliminating the temperature-dependent wire resistance from the measured complex transfer impedance so that a single probe can be used in a wide frequency range extending well over more than two decades [26].

As it was indicated at the beginning of Section 2, instrument calibration is achieved by transforming the actually measured complex electric impedance of the probe coil into a so-called AECC parameter in order to remove the influence of the measurement system. According to the standard 4-point linear interpolation procedure, four reference points are measured on two appropriate calibration blocks with and without a polymer foil of known thickness between the probe coil and the specimens. For the small conductivity variations considered in this study, sufficiently accurate results can be achieved by choosing two calibration blocks that closely bracket the conductivity range of interest. Then, the unknown AECC can be calculated from the complex coil impedance produced by the actual specimen using simple linear interpolation [19]. Because of the high precision requirements of these measurements, efficient rejection of the often inevitable lift-off variations is of the utmost importance. Unfortunately, spurious capacitance effects render the complex eddy current coil impedance variation with lift-off, the so-called lift-off curve, increasingly nonlinear at high frequencies. This nonlinearity makes it difficult to achieve accurate eddy current conductivity measurements using simple linear interpolation beyond 25 MHz. It was recently shown that the adverse effects of lift-off uncertainties on high-frequency AECC measurements can be very effectively reduced by nonlinear interpolation techniques [27].

This comparison illustrates how effectively the 4-point instrument calibration procedure separates the sought material effects associated with the peening from different measurement system parameters that also influence the measured probe coil impedance. In its simplest form, the 4-point instrument calibration method assumes a straight lift-off trajectory and uses linear interpolation, i.e., it accounts for the changing slope of the trajectory with both conductivity and

frequency, which makes it more suitable for precision measurements. Above 20 MHz, where inevitable lift-off variations adversely influence the accuracy of the AECC measurement, nonlinear interpolation must be used to achieve the same stringent requirements of about 0.1% relative accuracy.

2.3 AECC inversion

The measured frequency-dependent AECC must be inverted into a depth-dependent electric conductivity profile before it can be converted into the sought residual stress profile using the known piezoelectric parameter of the material. Because of the limited accuracy of both the AECC spectrum and the approximations used to relate conductivity to stress, a simplistic inversion technique will suffice in most cases [20]. According to this approach, at any given frequency the measured AECC corresponds roughly to the actual electric conductivity at half of the standard penetration depth. It might seem highly unlikely that such a simplistic inversion procedure could reasonably predict the actual conductivity profile from the measured frequency-dependent AECC, $\Gamma(f)$. Indeed, generally, this simplistic inversion method yields rather poor results. However, even in extreme cases, such as a rectangular profile representing a uniform layer of increased conductivity on a homogeneous substrate, the peak conductivity and half-peak penetration depth of the reconstructed profile are both well-reconstructed. When necessary, much more accurate inversion can be achieved by iterative application of the same principle in a feed-back loop that relies on the outstanding accuracy and speed of the 1D forward approximation of the electromagnetic problem [23]. The iterative in version technique is numerically stable as long as the random variations of the AECC spectrum remain below $\pm 0.1\%$. Beyond this level, the robustness of the iterative inversion procedure is adversely affected by random variations in the AECC spectrum. In such cases smoothening of the measured AECC profile can be used to eliminate potential inversion instabilities.

3. Measurement limitations

The main limitation of residual stress profiling by eddy current conductivity spectroscopy is that the feasibility of this technique seems to be limited to nickel-base superalloys, though some beneficial information, e.g., on increasing hardness, could be also obtained by this technique on titanium and aluminium alloys. Unfortunately, even in the case of nickel-base superalloys, there exist some serious limitations that adversely influence the applicability of the eddy current method. In this chapter, three such adverse effects will be reviewed. First, forged nickel-base superalloys often exhibit significant conductivity inhomogeneity that could interfere with subsurface residual stress characterisation. Second, these materials are susceptible to cold-work-induced microstructural changes that cause a conductivity increase similar or even larger than the primary conductivity increase caused by compressive residual stresses. Third, the electrical conductivity in nickel-base superalloys is rather low ($\approx 1.5\%$ IACS), therefore the standard penetration depth is relatively high at a given frequency ($\approx 180\,\mu$m at 10 MHz). Therefore, we cannot fully reconstruct the critical near-surface part of the residual stress profile in moderately peened components using only typical inspection frequencies below 10 MHz. In such cases, special high-frequency inspection techniques are needed to extend the frequency range up to 50–80 MHz, i.e., beyond the range of commercially available instruments.

3.1 Inhomogeneity effect

Surface-treated nickel-base superalloys exhibit an approximately 1% increase in AECC at high inspection frequencies, which can be exploited for nondestructive subsurface residual stress assessment. Unfortunately, microstructural inhomogeneity in certain as-forged and precipitation

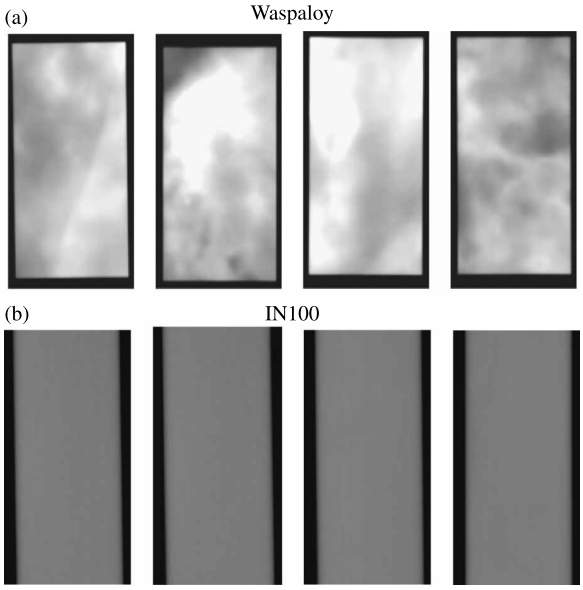

Figure 5. Examples of the AECC maps of unpeened inhomogeneous as-forged Waspaloy specimens (a) and homogeneous powder metallurgic IN100 specimens (b) at 6 MHz.

hardened nickel-base superalloys, like Waspaloy, can lead to significantly larger electrical conductivity variations of as much as 4–6%. Figure 5 shows examples of typical eddy current conductivity images from inhomogeneous Waspaloy specimens and homogeneous IN100 specimens taken at 6 MHz. The as-forged Waspaloy specimens were 53 × 107 mm and exhibited a wide conductivity range from 1.38 to 1.47% IACS, or ±3.2% in relative terms. In contrast, the 28 × 56 mm powder metallurgic IN100 specimens exhibited a very narrow conductivity range from 1.337 to 1.341% IACS or ±0.13% in relative terms. It should be mentioned that images of IN718 specimens revealed a medium level of inhomogeneity. It is postulated that the observed electrical inhomogeneity difference between Waspaloy, IN718, and IN100 is caused by their different alloy composition and thermo-mechanical processing and it is somehow related to the microstructure of these materials.

The roughly 3–4% electrical conductivity variation exhibited by inhomogeneous Waspaloy specimens raises a crucial question: Can eddy current techniques detect, let alone quantitatively characterise, the weaker near-surface conductivity variations caused by surface treatment in the presence of this much stronger conductivity inhomogeneity caused by microstructural variations? Eddy current conductivity images taken at different inspection frequencies indicated that low- and high-conductivity domains are essentially frequency independent due the large volumetric size of these domains [25]. This virtual frequency independence can be exploited to distinguish these inhomogeneities from near-surface residual stress and cold work effects caused by surface treatment, which, in contrast, are strongly frequency-dependent. As the frequency decreases, the eddy current penetrates deeper into the material and also spreads a little wider in the radial direction. Although there is some change in the AECC with frequency at most locations, on average this frequency-dependence essentially cancels out for a large number of points.

The rather weak frequency-dependence of the inhomogeneity-induced AECC variation suggests that the conductivity does not vary sharply with depth, which can be exploited

to separate the primary residual stress effect from the spurious material inhomogeneity using point-by-point absolute AECC measurements over a wide frequency range, followed by a comparison of the near-surface properties measured at high frequencies to those at larger depth measured at low frequencies. As an example, Figure 6 shows the cold work (a) and residual stress (b) profiles measured by XRD, the AECC spectrum (c), and the estimated residual stress profile (d) calculated from the measured AECC for as-forged Waspaloy specimens of four different peening intensities. Solid symbols represent as-peened specimens and empty symbols represent fully relaxed specimens after 24-h heat treatment at 900°C. In fact, in shot-peened specimens the excess AECC is roughly proportional to the peening intensity. Within the uncertainty of the eddy current measurement, the excess AECC completely vanished on fully relaxed specimens, which indicates that the eddy current method is indeed very sensitive to thermal relaxation. These results illustrate that the adverse effect of inhomogeneity can be separated from the primary residual stress effect using a self-referencing method based on the significant difference between the frequency-dependences of the residual stress and inhomogeneity contributions. The inherently increased experimental uncertainty associated with AECC spectra obtained from inhomogeneous specimens relative to homogenised Waspaloy specimens necessarily reduces the feasibility of precise residual stress assessment, but does not exclude it.

3.2 Cold work effect

Figure 6 indicates that the piezoresistivity effect is simply not high enough to account for the observed total AECC increase. For inversion purposes we used $\kappa_{ip} = -0.8$, which was

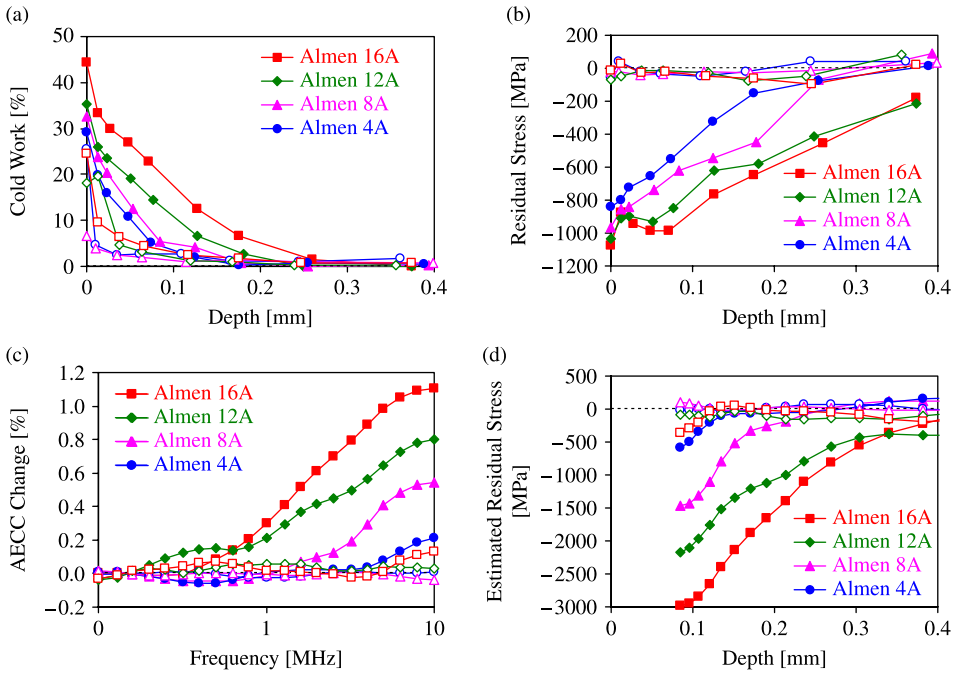

Figure 6. XRD cold work (a) and residual stress (b) profiles, AECC change (c), and the estimated residual stress profile (d) calculated from the measured AECC change for as-forged Waspaloy specimens of four different peening intensities. Solid symbols represent as-peened specimens and empty symbols represent fully relaxed specimens after 24-h heat treatment at 900°C.

measured on a reference specimen cut from the same batch of material. A comparison of the scales in Figure 6 (b, d) reveals that the inverted residual stress significantly overestimates the more reliable XRD results. It should be mentioned that the overestimation is much lower in IN718 and, especially, in IN100.

The most probable reason for the observed overestimation is the influence of cold work. In order to better understand the effects of cold work on the AECC change in shot-peened nickel-base superalloys, the effect of plastic deformation on the electrical conductivity, magnetic permeability, and electroelastic coefficient of premium grade rotor-quality nickel-base superalloys was investigated in detail [22]. The results indicated that, within the uncertainty of the measurement, the electroelastic coefficient and the magnetic permeability do not change as a result of cold work, therefore they cannot be responsible for the significant overestimation of the residual stress described above. On the other hand, the electric conductivity did show significant variation with plastic strain in cold-worked nickel-base superalloys. The substantial increase of the electrical conductivity is due to microstructural changes and could explain the observed residual stress overestimation. Of course, the cold work produced by SP rapidly decays away from the surface and the depth of the affected layer is typically only 30% of the thickness of the layer of compressive residual stress. Therefore, at frequencies below 10 MHz the overestimation tends to be less than what could be expected based on the sheer magnitudes of these two effects.

Cold work exerts a very convoluted effect on residual stress profiling by eddy current spectroscopic measurements and will require further research to better understand its behaviour and to develop possible compensation strategies. However, it should be pointed out that the overestimation of the eddy current method due to cold work is much lower in moderately peened components, which exhibit better thermo-mechanical stability, and in LSP and LPB specimens, which offer much lower plastic deformation than shot-peened ones. Figure 7 shows an example of comparison between eddy current and XRD results in low-plasticity burnished Waspaloy of approximately 15% maximum plastic strain. There is a fairly good agreement between the non destructive eddy current and destructive XRD residual stress profiles. However, the agreement in magnitude is somewhat artificial because we had to use $\kappa_{ip} = -1.2$ instead of the independently measured calibration value of $\kappa_{ip} \approx -0.8$ to eliminate the otherwise still significant overestimation by the eddy current method due to uncorrected cold work effects. It should be mentioned that, thanks to recent improvements in LPB technologies, the cold work level could

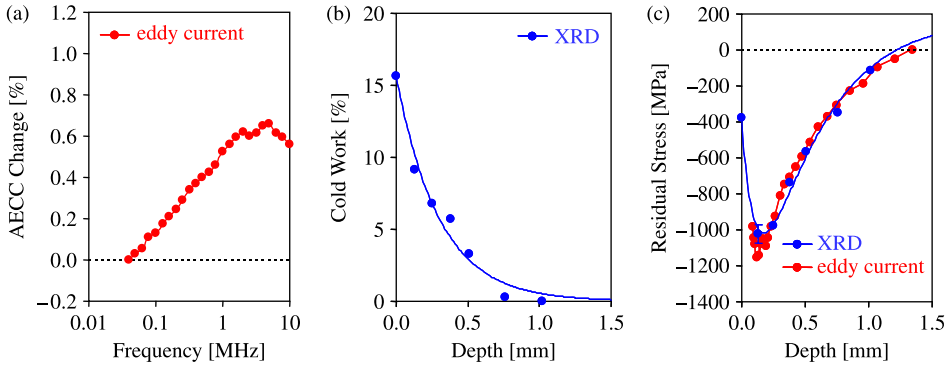

Figure 7. The measured AECC change (a), XRD cold work profile (b), and XRD versus inverted eddy current residual stress profiles (c) in low-plasticity burnished Waspaloy.

be reduced to less than 5%, which would further reduce the need for such empirical corrections that depend on material properties as well as on the type of surface treatment.

3.3 High-frequency inspection

The main reason for choosing peening intensities in excess of typical levels recommended by engine manufacturers in early studies was that the eddy current penetration depth could not be sufficiently decreased without extending the frequency range above 10 MHz, i.e., beyond the operational range of most commercially available eddy current instruments. In contrast, in the case of eddy current residual stress profiling in shot-peened nickel-base superalloys, the inspection frequency has to be extended to at least 50 MHz to capture the important part of the near-surface residual stress profile. For this purpose, we adapted an Agilent 4294A high-precision impedance analyser to eddy current conductivity spectroscopy [26]. The eddy current system based on this instrument offers better stability, reproducibility, and measurement speed than the formerly used commercial eddy current instruments. Spiral coils made on polymer foils offer high resonance frequency, thereby making them suitable for operation at high inspection frequencies [41,42]. Using separate transmit and receive coils improves the probe coil's thermal stability by eliminating the temperature-dependent coil resistance from the measured electric impedance.

Unfortunately, spurious capacitive effects render the lift-off trajectory of the probe coils more nonlinear at high frequencies and make it rather difficult to achieve accurate AECC measurements above 25 MHz [27]. The inductive and capacitive effects on the lift-off sensitivity of the probe coil are opposite. The inductive effect dominates below 20 MHz, i.e., at typical eddy current inspection frequencies. Both effects increase with frequency with the inductive effect being initially stronger, but then it is taken over at high frequencies by the faster growing capacitive effect. Since the two effects produce opposite curvature in the lift-off trajectory, in the frequency range where they are approximately equal the lift-off trajectory becomes essentially linear and very accurate conductivity measurements can be conducted even in the presence of substantial lift-off variations.

To reduce the spurious dependence of AECC measurements on inevitable random lift-off variations at high inspection frequencies, a nonlinear interpolation method was introduced [27]. The efficiency of this approach is illustrated in Figure 8 which shows the experimentally

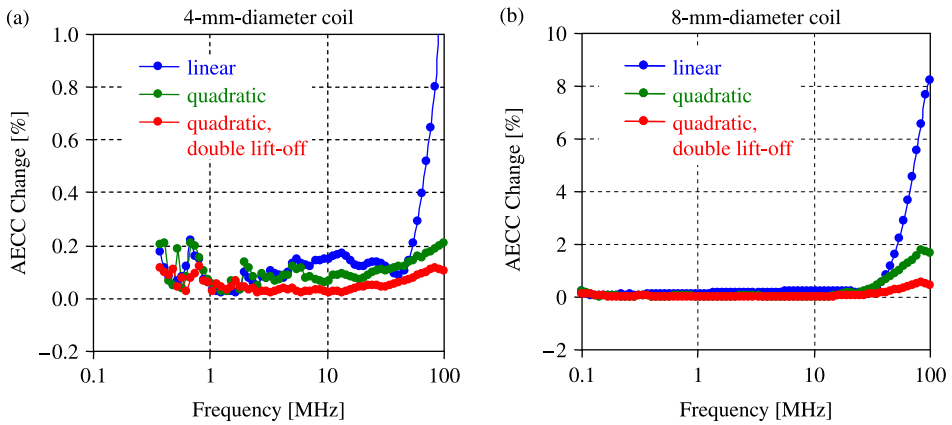

Figure 8. Experimentally determined lift-off sensitivity versus frequency for 4-(a) and 8-mm diameter(b) coil sizes.

determined lift-off sensitivity versus frequency for 4- and 8-mm diameter coils. In this paper, these flat spiral coils are referred to simply by their outer diameter, which is exactly twice their inner diameter. The width of the conducting strip and the air gap between neighbouring turns was kept constant at 0.1 mm. Computational simulation was conducted to study the sensitivity of these coils using the commercially available Vic-3d program [27]. The simulations were found to be in good agreement for the conductivity sensitivity over the whole frequency range from 0.1 to 100 MHz and for the lift-off sensitivity from 0.1 MHz up to about 20 MHz. At higher frequencies the lift-off sensitivity becomes a crucial issue that can compromise the accuracy of conductivity measurements in the presence of lift-off uncertainties as small as 0.05 mm. Above 20 MHz, the purely inductive Vic-3D simulation greatly underestimated the experimentally observed lift-off sensitivity of these probe coils. It was shown that the increasing susceptibility of conductivity measurements to lift-off variations is due to capacitive effects that are not accounted for in the simulation. Therefore, a simple lumped-element analytical simulation was suggested to better understand the underlying physical phenomenon [27]. Further research is needed to develop numerical tools that properly incorporate self- and stray-capacitance effects into the eddy current simulation.

Figure 8 illustrates that the lift-off rejection is much better for the smaller probe (the vertical scales are different by a factor of 10) and when quadratic interpolation is used for instrument calibration. Furthermore, in the latter case, the rejection can be further improved by extending the calibration lift-off range since the curvature is more accurately measured over a larger distance. In contrast, in the case of linear interpolation the lift-off rejection decreases with increasing lift-off calibration range.

To illustrate the advantages of high-frequency conductivity spectroscopy, Figure 9 shows the cold work (a) and residual stress (b) profiles obtained by destructive XRD measurements in shot-peened IN100 specimens of Almen 4A, 8A, and 12A peening intensities. For comparison purposes, Figure 9(b) also shows the residual stress profiles reconstructed from the measured AECC spectra. Except for a sharper-than-expected near-surface 'hook' observed in the Almen 8A specimen, which is most probably caused by imperfect lift-off rejection above 25 MHz, the general agreement between the AECC and XRD data is very good. In the first step, the depth-dependent electric conductivity change was calculated using the previously described iterative inversion procedure [23]. Then, the sought depth profile of the residual stress was estimated by neglecting cold work and surface roughness effects. In order to get the good overall agreement illustrated in Figure 9(b), we had to use a corrected value of $\kappa_{ip} = -1.06$, which is 33% lower

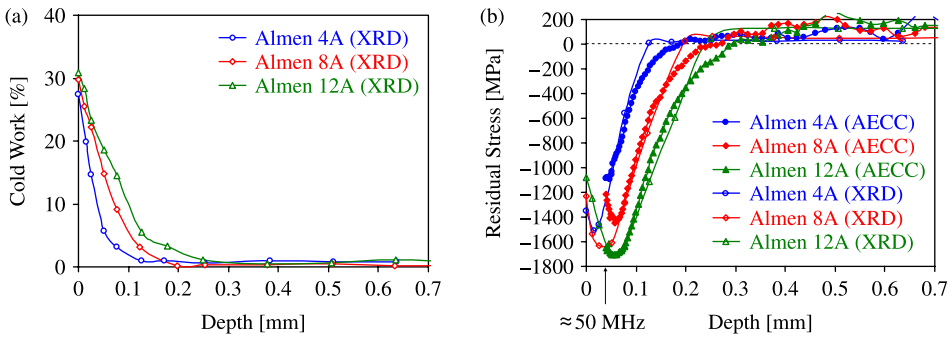

Figure 9. XRD profiling of near-surface cold work (a) and residual stress (b) profiles compared to the inverted eddy current residual stress profile in shot peened IN100 specimens of Almen 4A, 8A, and 12A peening intensity levels.

than the independently measured average value for IN100. The exact reason for the need for this 'empirical' correction is currently not known and will require further investigation. However, it should be pointed out that the present underestimation of the residual stress level by the inverted AECC relative to the destructive XRD results does not seem to be physically related to the above described overestimation in Waspaloy and IN718 alloys due to increasing electric conductivity caused by microstructural changes under extensive cold work. Since a single constant was sufficient to bring all the AECC and XRD results into good agreement with each other for all three peening intensities in spite of their different levels of cold work, the cause of this apparent

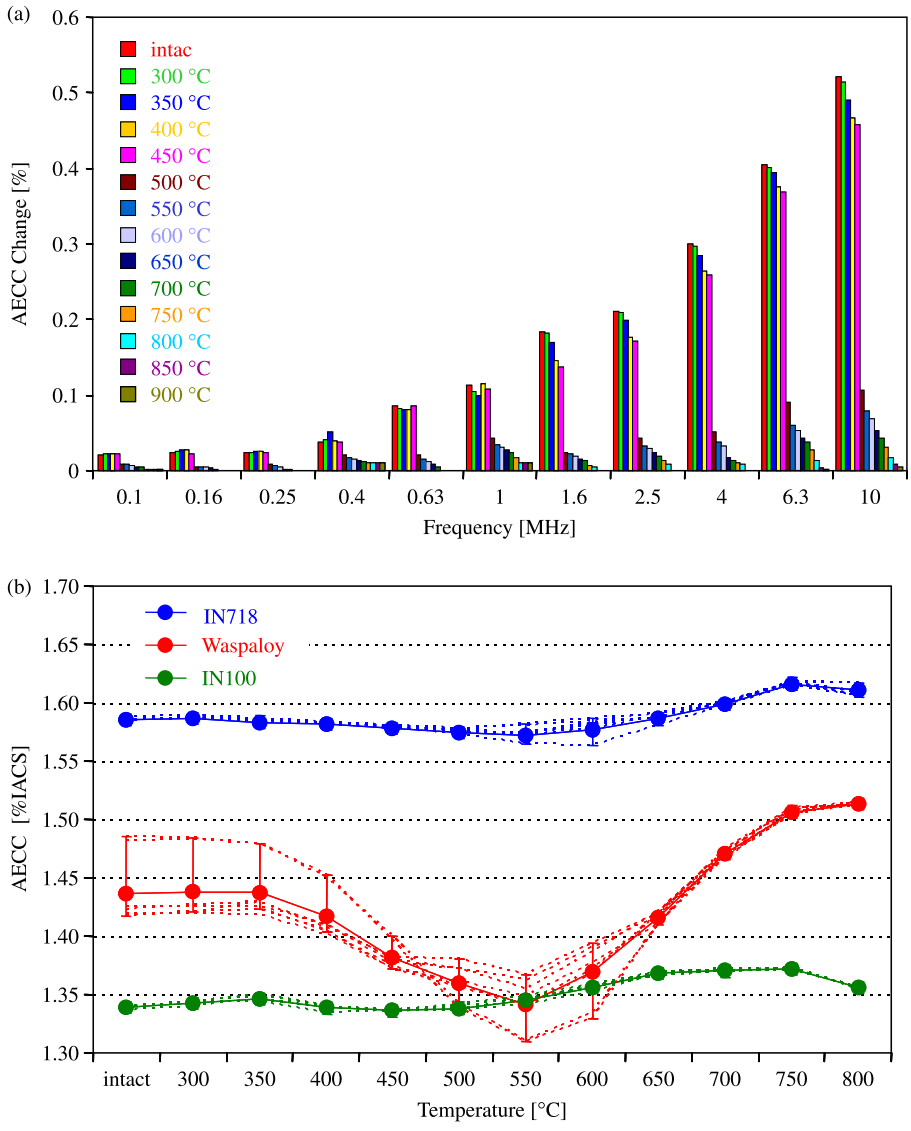

Figure 10. The decay of AECC change between the peened and unpeened parts of a Waspaloy specimen of Almen 8A peening intensity during gradual thermal relaxation (a) and the evolution of AECC in three nickel-base superalloys during gradual thermal exposure (b). Error bars indicate the range covered by eight specimens chosen from the same lot of each material.

underestimation by the AECC method is most probably the intrinsic variation of the electroelastic with microstructure.

4. Materials limitations

Previous experimental observations indicated that the sensitivity of eddy current conductivity spectroscopy is fairly low, but still sufficient for residual stress profiling in certain surface-treated engine alloys. However, the electrical conductivity and its stress-dependence are rather sensitive to microstructural variations, therefore the selectivity of this method leaves much to be desired. Recent research revealed a series of situations where anomalous stress-dependence and relaxation behaviour were observed. This is not surprising at all in the case of an inherently indirect non destructive method and should not lead to abandoning the eddy current approach, especially since no better alternative is known at this point. This chapter reviews four previously unreported recent experimental observations of anomalous materials behaviour and proposes further research efforts to better understand the underlying physical mechanisms and to mitigate the adverse influence of these phenomena on eddy current residual stress profiling.

4.1 Anomalous relaxation in Waspaloy

One of the main questions concerning the feasibility of eddy current residual stress profiling is whether the AECC difference decays gradually with thermal relaxation or not, which is extremely important from the point of view of assessing partial relaxation. Initial experimental evidence indicated that the decay is usually monotonic and gradual, but it was noticed early on that occasionally the rate of decay was much faster than expected. For example, in one of the first such experiments a Waspaloy specimen of Almen 8A peening intensity was gradually relaxed by repeated heat treatments of 24 h each at increasing temperatures in 50°C steps from 300 to 900°C in a protective nitrogen environment [19]. Figure 10(a) shows the observed AECC difference between the peened and unpeened parts after each heat treatment. These results clearly indicate that the measured AECC difference gradually decreases during thermal relaxation and almost completely disappears after the 13th 24-h heat treatment at 900°C. However, there was a very steep drop in the AECC difference at 450°C, which is highly suspicious as the peening-induced residual stress is certainly more persistent in Waspaloy at such a low temperature.

Subsequent studies investigated the changing electric conductivity of nickel-base superalloys due to microstructural evolution at elevated temperatures [25]. Figure 10(b) shows the evolution of the electrical conductivity in these three nickel-base superalloys (IN718, Waspaloy, IN100) during gradual thermal exposure. By far the strongest initial inhomogeneity among these materials was observed in Waspaloy. It was also noted that the electric conductivity significantly dropped between 400 and 500°C before it started to increase above 550°C. These results suggested that spurious electric conductivity variations caused by microstructural anomalies in nickel-base superalloys interfere with eddy current residual stress assessment of subsurface residual stresses. If the conductivity variations were entirely volumetric effects, they would not cause frequency-dependent changes in the AECC spectrum, therefore they could be distinguished from near-surface residual stress and cold work effects caused by surface treatment, which, in contrast, are strongly frequency-dependent. According to the self-referencing method, the average AECC measured at sufficiently low frequencies (e.g., between 0.1 and 0.3 MHz) is subtracted from the absolute AECC measured at all frequencies, i.e., the conductivity close to the surface is compared to the conductivity at a sufficiently large depth where the material can be considered intact, i.e., unaffected by surface treatment.

Recent experimental observations indicate that the above assumption is not necessarily valid in Waspaloy specimens relaxed at around 400–450°C. Figure 11(a) illustrates schematically how the presence of cold work reduces the transition temperature at which thermally activated microstructural evolution takes place in the material. For example, let us assume that the typically 30–40% near-surface plastic strain caused by cold work reduces the activation temperature by about 40°C. If then the surface-treated component is exposed to moderate temperatures so that the transition occurs in the cold-worked near-surface layer, but not deeper below the surface, a significant conductivity difference will develop, as it is shown in Figure 11(b). This effect will be detectable in the measured frequency-dependent AECC spectrum and could easily overshadow the residual stress relaxation effect that is very weak at these temperatures. Currently, experiments are underway to verify that the steep drop illustrated in Figure 10(a) would actually reach below zero if the exposure time were increased. The most obvious way to mitigate this problem seems to be to expose all the new components to a carefully chosen heat treatment, e.g., 500–550°C for 24 h. Such treatment would significantly reduce further changes in conductivity and might not be necessary at all on used components which tend to develop a uniformly high electric conductivity distribution due to their long exposure to elevated operational temperatures.

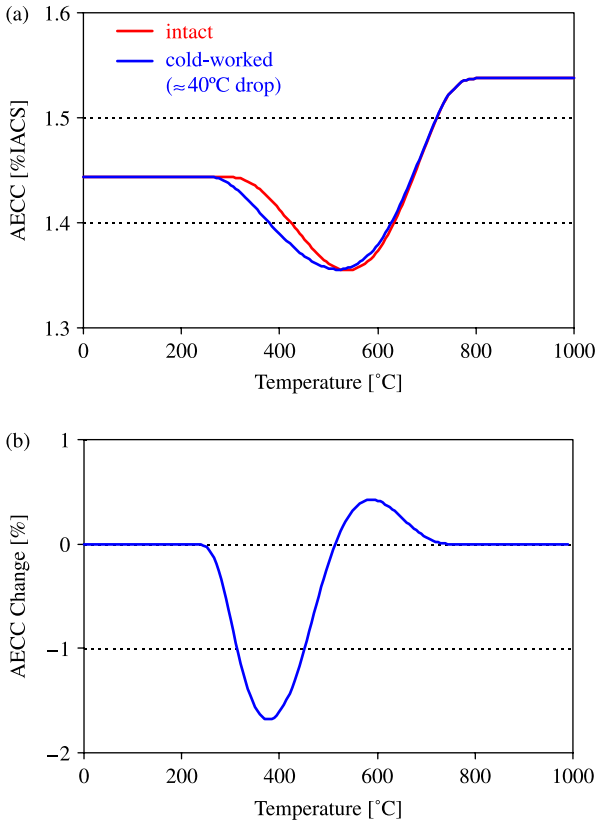

Figure 11. A schematic illustration of how the presence of cold work reduces the transition temperature at which thermally activated microstructural evolution takes place in the material (a) and the resulting AECC change between the cold-worked surface and the intact interior (b).

4.2 Anomalous behaviour in hardened IN718

It was recently found that special versions of the common IN718 material can also exhibit anomalous behaviour that is very different from those of the commercial versions reported in the literature [19,22,25,28]. A common feature of these materials seems to be that their custom-designed thermo-mechanical processing results in both increased hardness and increased electric conductivity. Figure 12 shows examples of AECC spectra measured in Honeywell Engines DP718 specimens which were shot-peened to Almen 6A intensity and 200% coverage. The curved specimen (OD = 50.8 mm and ID = 34.9 mm) shown in Figure 12(a) was machined from hot rolled material and behaved conventionally, i.e., the AECC increased with frequency by approximately 1–2%. It should be mentioned that the significant difference between these spectra above 25 MHz indicates uncorrected curvature effects. In comparison, the AECC spectra measured on the two flat specimens machined from the first batch of forged material exhibit a much smaller increase in conductivity at high frequencies, which is not compatible with previous measurements on IN718 and the electroelastic coefficient independently measured on DP718. Although the reason for this discrepancy is not understood at present, it seems to be related to the microstructural differences between the two materials. For example, it was reported in the literature before that soft fully annealed Waspaloy produced a much stronger AECC increase at high frequencies than harder as-forged Waspaloy [25].

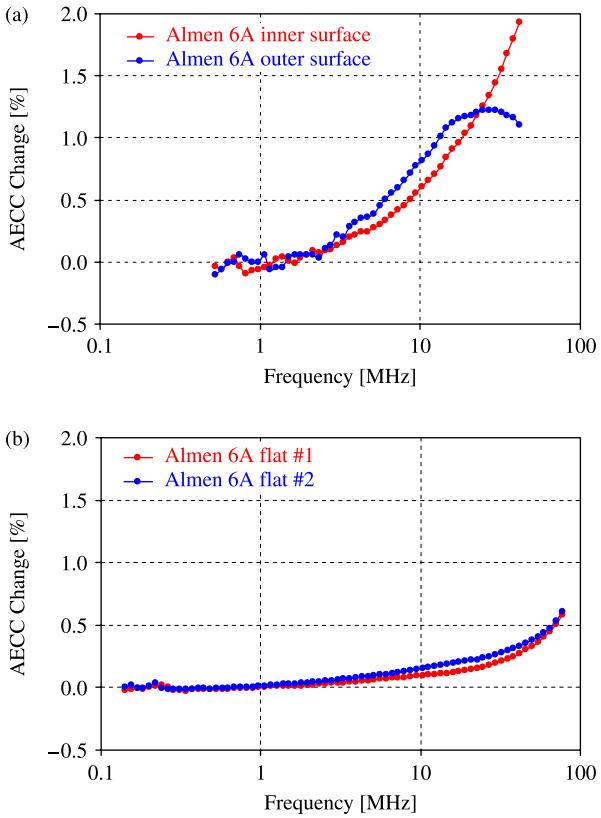

Figure 12. Examples of AECC change measured in Honeywell Engines DP718 specimens shot-peened to Almen 6A intensity. The curved specimen (OD = 50.8 mm and ID = 34.9 mm) was machined from hot rolled material (a) while the two flat specimens were machined from forged material (b).

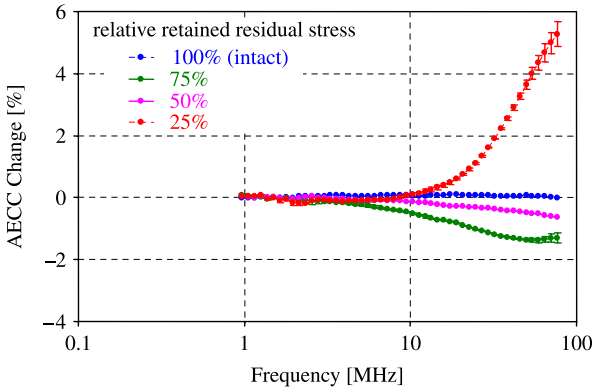

Figure 13. AECC change versus frequency measured in a second batch of flat forged DP718 specimens of Almen 6A peening intensity and 200% coverage after thermal relaxation resulting in different relative levels of retained peak residual stress.

Preliminary results in DP718 indicate that the AECC spectrum is much more variable from batch to batch than in ordinary IN718 and it exhibits very strange non-monotonic thermal relaxation behaviour, most probably because of presently poorly understood thermally activated microstructural evolution. Four flat DP718 specimens of Almen 6A peening intensity and 200% coverage were prepared for this part of the study by Honeywell Engines from a second batch of forged material. Subsequently, the peak residual stress in three of these specimens was reduced to 75, 50, and 25% of the original as-peened level using well-controlled thermal relaxation. Subsequently, four AECC measurements were conducted at different spots on each specimen and the results were averaged. Figure 13 shows the AECC change as a function of frequency for these four specimens. No unique trend can be identified from these results that would correlate the measured AECC change to the residual stress profiles obtained by XRD. In addition, the AECC change produced in the second batch of forged DP718 peened under the same nominal conditions was much less than in the unexpectedly small but still detectable AECC increase observed in the first batch. The results shown in Figure 13 are very surprising and not properly understood. Further research is needed to understand why DP718 specimens prepared from forged stock seem to behave so differently from other nickel-base superalloys tested in earlier

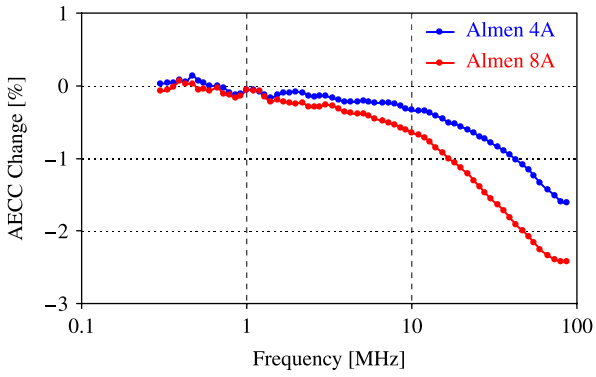

Figure 14. Examples of AECC change measured in two MTU IN718 specimens shot-peened to different intensities.

studies, when a monotonic correlation between the XRD and AECC results was found. At this point, the only potentially significant difference we found between DP718 and ordinary IN718 is the perceivably higher electric conductivity ≈1.64% IACS of the former versus 1.38–1.56% IACS for the latter. The parallel and normal electroelastic coefficients of DP718 were determined following the earlier developed procedure [21]. Based on these measurements we found that the isotropic plane stress electroelastic coefficient of DP718 is $\kappa_{ip} \approx -1.22$, fairly similar to the $\kappa_{ip} \approx -1.54$ average value found for IN718, which also excludes the possibility that the observed anomalous behaviour is residual stress related.

Interestingly, a similar, and probably related, effect was observed recently in custom-treated IN718 provided by MTU of Munich, Germany. Figure 14 shows the AECC spectra measured in two MTU IN718 specimens shot-peened to different intensities. These results represent the very first observation of negative rather than positive AECC change in any as-peened nickel-base superalloy. The specific microstructural differences between the MTU version of IN718 and other commercially available versions are presently not known except that the former exhibits perceivably higher electric conductivity ≈1.58–1.63% IACS versus 1.38–1.56% IACS and also significantly higher Vickers hardness around 460 HV versus 260 HV for commercial IN718 (Hillmann, S. and Meyendorf, N., Private Communication, 2008). The role of different thermo-mechanical processing on the AECC signature of surface-treated components

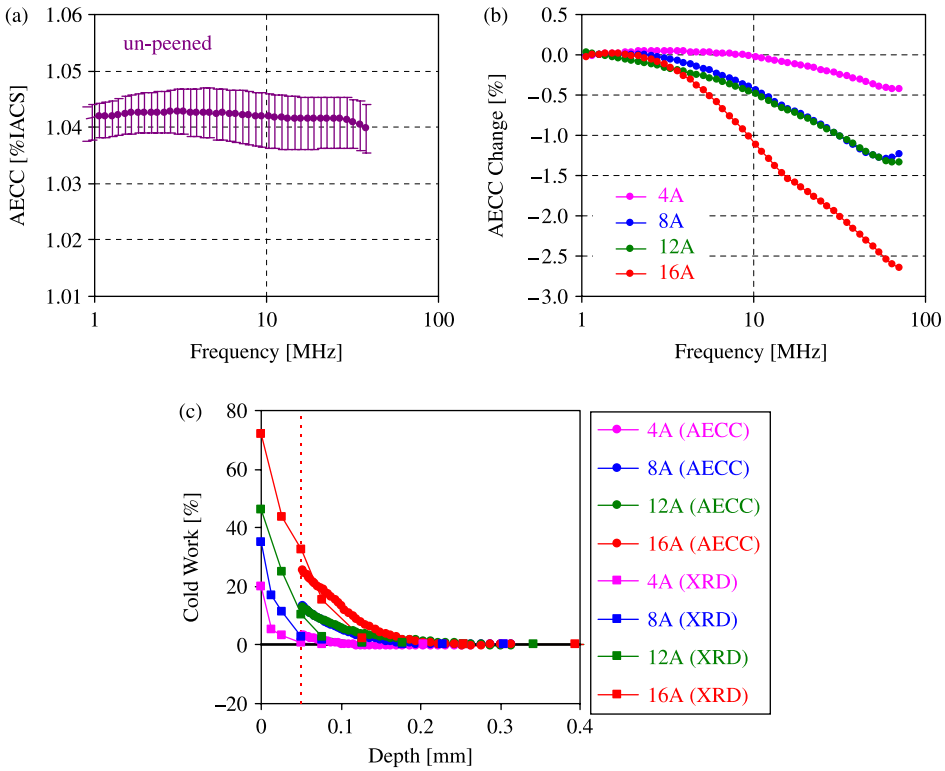

Figure 15. Absolute AECC measurements on the un-peened (a), relative AECC change measurements on the shop-peened (b) sides of Ti-6A1-4V, and comparison between XRD and eddy current cold work profiles (c). Error bars indicate the range covered same lot of the material.

is currently being investigated at the Fraunhofer Institute for NDT in Dresden, Germany, and the findings of that study will be published later.

4.3 Profiling in surface-treated Ti–6Al–4V

Initially, Ti–6Al–4V was one of the first materials tested for eddy current residual stress 20 characterisation [11,14]. However, later this interest faded away when it was found that in Ti–6Al–4V the electric conductivity is insensitive to isotropic plane stress, as it was illustrated in Figure 2. Because of direct exposure to erosion and foreign body impact damage, NDE of low-temperature inlet fan and compressor blades, which are usually made of titanium alloys, is even more important than that of high-temperature turbine components downstream, which are usually made of nickel-base superalloys. Therefore, reliable engine rotor life prognostics absolutely requires that an eddy current, or other suitable NDE method be developed for near-surface cold work characterisation in titanium alloy components.

One of the main reasons why titanium alloys were originally thought to be less promising candidates for eddy current inspection is that they dominantly crystallise in hexagonal symmetry and therefore exhibit significant texture-induced electric anisotropy on the order of 3–4% relative conductivity variation in a highly textured Ti–6Al–4V plate [39]. Our initial measurements on shot-peened Ti–6Al–4V indicated a decrease in apparent eddy conductivity near the surface [19]. Since the stress-dependence of electric conductivity is almost negligible in Ti–6Al–4V and the surface roughness induced AECC loss is also negligible below 20 MHz, it was recently suggested that eddy current conductivity spectroscopy is selectively sensitive to crystallographic and morphological texture in the shot-peened Ti–6Al–4V and it might be exploited for near-surface cold work profiling [43].

Figure 15(a) shows the average of AECC measurements taken on the un-peened sides of four Ti–6Al–4V specimens. In spite of the significant point-to-point variation of conductivity, these results indicate that the average base-line conductivity spectrum is essentially frequency-independent up to 40 MHz, which illustrates that spatial averaging can sufficiently reduce the adverse inhomogeneity effect on AECC measurements. For this reason, spatial averaging was conducted on the peened sides as well. Figure 15(b) illustrates the average AECC change measured at four locations clustered around the centre on the peened side of four specimens peened at four different intensities. These results indicate that increasing the peening intensity level increases the drop in AECC measurements with frequency. However, there is a virtual overlap between the AECC change of the Almen 8A and 12A specimens. To check the reproducibility of these results, other specimens of Almen 8A and 12A from the same batch were tested and the results were found to be consistent in terms of AECC change even though they correspond to slightly different near-surface residual stress and cold work profiles.

Since near-surface cold work is the dominant factor affecting the AECC change in shot-peened Ti–6Al–4V, the AECC change can be correlated to the presence of cold work alone through an empirically determined dimensionless isotropic plane electroplastic coefficient [43]. Figure 15(c) shows a comparison between XRD and eddy current cold work profiles. The frequency-dependent AECC change was first inverted to a depth-dependent electric conductivity profile using the simplistic inversion technique [20]. Then, the depth-dependent conductivity change was converted into the near-surface cold work profile assuming a dimensionless isotropic plane electroplastic coefficient of -0.08 which was determined by best fitting of the inverted eddy current results to the near-surface cold work profiles obtained by destructive XRD measurements. The recently developed iterative inversion technique could not be used due the sharp change in the depth-dependent conductivity profile within a short distance below the surface [23]. However, the results using the more robust simplistic inversion technique

indicate the possibility of using AECC measurements for near-surface cold work profiling in shot-peened Ti–6Al–4V.

5. Conclusions

This paper dealt with nondestructive characterisation of near-surface residual stress caused by plastic deformation during surface treatment. Residual stress causes remnant elastic strain, i.e., change in lattice separation, even in the absence of external applied loads. Surface treatments aim at producing compressive subsurface residual stresses that can significantly extend the fatigue life of fracture–critical components. Depending on how the plastic deformation was achieved by cold work, e.g., by SP, LSP, or LPB, surface treatment also leaves substantial microstructural damage behind in the material. The degree of cold work is often characterised simply by the amount of plastic strain produced in the material. Although cold work might have some beneficial effects on the material, such as surface hardening, in most cases it affects adversely the material. In particular, cold-work-induced microstructural damage is largely responsible for the accelerated thermal relaxation of protective residual stress in surface-treated components. In most engine materials, this adverse effect of cold work becomes especially strong above 10% equivalent plastic strain, which is why SP, that produces as much as 20–40% plastic strain at the surface, is so inefficient on critical components operating at elevated temperatures. The potential of thermal relaxation at elevated operational temperatures necessitates repeated checks during periodic maintenance. Since, existing inspection methods either cannot be applied to subsurface residual stress assessment or are destructive in nature, new nondestructive characterisation methods are being sought to replace them. Eddy current conductivity spectroscopy has emerged as one of the leading candidates for non-destructive residual stress profiling in surface-treated metals. This is an experimental method that will require further research before it can be applied in field inspection. Currently, its feasibility for quality monitoring during manufacturing and assessing subsequent relaxation during service has been demonstrated only for certain nickel-base superalloys. The main limitation of residual stress profiling by eddy current conductivity spectroscopy is that, although the method is sensitive enough to weak elastic strains to be practically useful, it is not sufficiently selective for them. Even for the limited range of nickel-base superalloys numerous limitations have been identified in the literature, such as spurious inhomogeneity in some forged engine alloys, interference from cold-work-induced microstructural damage, and practical inspection difficulties associated with the very high inspection frequencies required to capture the peak compressive stress in moderately shot-peened components. Because of the aforementioned limitations, eddy current conductivity spectroscopy cannot be expected to replace XRD residual stress measurements. However, because of its relative simplicity and nondestructive nature, it might supplement this more accurate but destructive XRD technique.

This paper discussed numerous recently discovered additional materials limitations that are presently not properly understood. The presented experimental evidence indicates that the excess AECC in surface-treated nickel-base superalloys is due in part to elastic strains, i.e., residual stress, and in part to plastic strains, i.e., cold work, and it is also adversely influenced by thermally or thermo-mechanically activated microstructural changes. The very fact that the conductivity increases rather than decreases was originally thought to indicate that the observed AECC increase was mainly due to the presence of compressive residual stresses. This assumption was also supported by XRD results on fully relaxed specimens showing that the cold work induced widening of the diffraction beam only partially vanishes when both the residual stress and the AECC completely disappear due to thermal relaxation.

Phase transformations can occur in nickel-base superalloys parallel to residual stress relaxation at normal operational temperatures of engine components. There is mounting evidence that in the presence of plastic deformation damage thermal exposure can lead to accelerated microstructure evolution which causes conductivity changes that interfere with, and sometimes even overshadow, direct indications of the residual stress and cold work effects caused directly by the surface treatment. Experimental observations first reported in this paper indicate that some of these crucial materials issues have not been solved sufficiently for this technique to be adopted for field applications yet and further research is needed to better understand the underlying physical phenomena and the influence of materials variations. Although we did not measure the chemical composition of our nickel-base superalloy specimens, they all complied with tight tolerances specified for such engine materials. Based on our most recent observations, referring to these materials by their commercial name and general thermomechanical processing (fully annealed, hot rolled, forged, precipitation hardened, etc.) might not be sufficient for the purposes of understanding the specific behaviour exhibited by these materials. One of the main goals of this paper was to draw attention to the need for further research of the unresolved materials issues. Specifically, additional research is needed to better understand the correlation between hardness and electroelastic/electroplastic behaviour in these materials.

Acknowledgments

This work was supported by the Air Force Research Laboratory partly under Contract No. F33615-03-2-5210 with the University of Cincinnati and partly through the Quantitative Inspection Technology for Aging Military Aircraft program with Iowa State University on delivery order number 5007-IOWA-001 of the prime contract F09650-00-D-0018. Additional support was provided through cooperation with the Center for NDE at Iowa State University with funding from the Air Force Research Laboratory on contract FA 8650-04-C-5228. The diffraction measurements reported in this study were made by Lambda Research of Cincinnati. The authors would like to acknowledge valuable discussions and ongoing collaboration with Susanne Hillmann and Norbert Meyendorf of the Fraunhofer Institute for NDT in Dresden, Germany.

Notes

1. General Electric Aviation, Cincinnati, OH 45215, USA.
2. Cessna Aircraft, Wichita, KS 67277, USA.
3. Rolls-Royce Corporation, Indianapolis, IN 46241, USA.

References

[1] V. Hauk, *Structural and Residual Stress Analysis by Nondestructive Methods*, Elsevier, Amsterdam, Netherlands, 1997.
[2] J.T. Cammett, P.S. Prevéy, and N. Jayaraman, *Proceedings of ICSP 9*, Marne-la-Vallee, Paris, France, 2005.
[3] P.S. Prevéy, *IITT-International*, Gournay-Sur-Marne, France (1990), p. 81.
[4] D.J. Hornbach, P.S. Prevéy, and M. Blodgett, *Review of Progress in Quantitative NDE*, Vol. 24, American Institute of Physics, Melville, NY, 2005, pp. 1379–1386.
[5] M.G. Moore and W.P. Evans, *Mathematical Correction for Stress in Removal Layers in X-ray Diffraction Residual Stress Analysis*. SAE Trans. 66 (1958), pp. 340–345.
[6] M. Francois, F. Convert, and J. Lu, *'X-Ray Diffraction Method' Handbook of Measurement of Residual Stresses*, Society of Experimental Mechanics, Fairmont Press, Lilburn, GA, 1996, pp. 71–132.
[7] G. Maeder, M. Barral, J.L. Lebrun, and J.M. Sprauel, Rigaku J. 3 (1986), pp. 9–21.
[8] A. Pyzalla, J. Nondestr. Eval. 19 (2000), pp. 21–31.

[9] N. Goldfine, *41st Army Sagamore Conference*, Plymouth, MA, 1994.
[10] N. Goldfine, D. Clark, and T. Lovett, *EPRI Topical Workshop: Electromagnetic NDE Applications in the Electric Power Industry*, Charlotte, NC, 1995.
[11] F.C. Jr. Schoenig, J.A. Soules, H. Chang, and J.J. DiCillo, Mater. Eval. 53 (1995), pp. 22–26.
[12] M. Blaszkiewicz, L. Albertin, and W. Junker, Mater. Sci. Forum 210 (1996), pp. 179–186.
[13] N. Goldfine and D. Clark, *EPRI Balance of plant heat exchanger NDE Symposium*, Jackson, WY, 1996.
[14] H. Chang, F.C. Jr. Schoenig, and J.A. Soules, Mater. Eval. 57 (1999), pp. 1257–1260.
[15] I. Lavrentyev, P.A. Stucky, and W.A. Veronesi, *Review of Progress in Quantitative NDE*, Vol. 19, American Institute of Physics, Melville, NY, 2000, pp. 1621–1628.
[16] J.M. Fisher, N. Goldfine, and N. Zilberstein, *49th Defense Working Group on NDT*, Biloxy, MS, 2000.
[17] V. Zilberstein, Y. Sheiretov, A. Washabaugh, Y. Chen, and N. Goldfine, *Review of Progress in Quantitative NDE*, Vol. 20, American Institute of Physics, Melville, NY, 2001, pp. 985–995.
[18] V. Zilberstein, M. Fisher, D. Grundy, D. Schlicker, V. Tsukernik, V. Vengrinovich, N. Goldfine, and T. Yentzer, J. ASME, Pressure Vessel Technol. 124 (2002), pp. 375–381.
[19] M.P. Blodgett and P.B. Nagy, J. Nondestr. Eval. 23 (2004), pp. 107–123.
[20] F. Yu and P.B. Nagy, J. Appl. Phys. 96 (2004a), pp. 1257–1266.
[21] ———, J. Nondestr. Eval. 24 (2005), pp. 143–152.
[22] ———, J. Nondestr. Eval. 25 (2006), pp. 107–122.
[23] B.A. Abu-Nabah and P.B. Nagy, NDT&E Int. 39 (2006), pp. 641–651.
[24] N. Nakagawa, C. Lee, and Y. Shen, *Review of Progress in Quantitative NDE*, Vol. 25, American Institute of Physics, Melville, NY, 2006, pp. 14718–1425.
[25] F. Yu, M.P. Blodgett, and P.B. Nagy, J. Nondestr. Eval. 25 (2006), pp. 17–28.
[26] B.A. Abu-Nabah and P.B. Nagy, NDT&E Int. 40 (2007a), pp. 405–418.
[27] ———, NDT&E Int. 40 (2007b), pp. 555–565.
[28] Y. Shen, C. Lee, C.C. H. Lo, N. Nakagawa, and A.M. Frishman, J. Appl. Phys. 101 (2007), p. 014907.
[29] M.P. Blodgett, C.V. Ukpabi, and P.B. Nagy, Mater. Eval. 61 (2003), pp. 765–772.
[30] K. Kalyanasundaram and P.B. Nagy, NDT&E Int. 37 (2004), pp. 47–56.
[31] F. Yu and P.B. Nagy, J. Appl. Phys. 95 (2004b), pp. 8340–8351.
[32] C.S. Smith, *Solid State Physics, Advance in Research and Application*, Vol. 6, Academic, New York, NY, 1958, pp. 175–249.
[33] M. Bao and Y. Huang, J. Micromech. Microeng. 14 (2004), pp. 332–334.
[34] E. Barsis, E. Williams, and C. Skoog, J. Appl. Phys. 41 (1970), pp. 5155–5162.
[35] Z. Rosenberg, D. Yaziv, and Y. Partom, J. Appl. Phys. 51 (1980), pp. 4790–4798.
[36] Y. Partom, D. Yaziv, and Z. Rosenberg, J. Appl. Phys. 52 (1981), pp. 4610–4616.
[37] D.Y. Chen, Y.M. Gupta, and M.H. Miles, J. Appl. Phys. 55 (1984), pp. 3984–3993.
[38] Y. Partom, Z. Rosenberg, and B. Keren, J. Appl. Phys. 56 (1984), pp. 552–553.
[39] M.P. Blodgett and P.B. Nagy, Appl. Phys. Lett. 72 (1998), pp. 1045–1047.
[40] N.J. Goldfine, Mat. Eval. 51 (1993), pp. 396–405.
[41] R.J. Ditchburn, S.K. Burke, and M. Posada, J. Nondestr. Eval. 22 (2003), pp. 63–77.
[42] R.J. Ditchburn and S.K. Burke, NDT&E Int. 38 (2005), pp. 690–700.
[43] B.A. Abu-Nabah and P.B. Nagy, *Review of Progress in Quantative NDE*, Vol. 27, American Institute of Physics, Melville, NY, 2008, 1228–1235.